



TUTORED PROJECT
M2 GEOPHYSICS

Modelling of the elastic deformation due to the Dead Sea water mass loss and comparison with geodetic data.

INSTITUT DE PHYSIQUE DU GLOBE DE PARIS, UNIVERSITÉ PARIS CITÉ

Students
Emile DENISE
Dingyan LI

Supervisors
Kristel CHANARD
Manon DALAISON

November 2024 - January 2025

Abstract

The Dead Sea water level has been decreasing by 40 m since 1960, and it has dropped at an average rate of 0.9 m.yr^{-1} since 1980. The decline in the Dead Sea's water level is mainly driven by anthropogenic factors. It has significant environmental implications, including subsidence, sinkhole formation, lithospheric rebound and regional uplift. Using an elastic half-space model, we predict deformation patterns resulting from hydrological unloading. We predict surface displacements of a few millimeters near the Dead Sea. These predictions are compared against geodetic data from InSAR and GNSS measurements to evaluate the model's accuracy. Results indicate that while the elastic model captures most aspects of observed deformation, it fails to fully explain the data. The findings highlight the need to incorporate additional factors to better understand crustal responses.

Table of contents

Abstract	2
Table of contents	2
Introduction	3
Methodology	4
Modelling hydrological elastic deformation	4
Extraction of geodetic displacement	5
Results	5
Discussion	10
Conclusion and perspectives	10
Acknowledgements and reproducibility	11
References	11
Appendices	13
A Discretization of the Dead Sea geometry	13
B Description of the InSAR data	13
C Displacement time series at GNSS stations	15

Introduction

The Dead Sea is a hypersaline endorheic lake situated at the lowest point on Earth's surface, which has experienced significant water mass loss over recent decades mainly due to anthropogenic factors (Closson et al., 2013). The Dead Sea is located on the border between Jordan, Israel and the West Bank. It is mainly fed by the Jordan River, which comes from the Sea of Galilee further north (Figure 1.a). The drainage basin of the dead Sea spans over Jordan, Israel, Palestinian territories, Syria and Lebanon and includes major cities such as Jerusalem or Amman. About 16 million people are consuming fresh waters that move towards the Dead Sea. The Dead Sea lies on a transform fault boundary – called the Dead Sea Transform – between the Arabian Plate and the African Plate (more specifically, the Sinai microplate). This left lateral-moving transform fault extends from the northern Red Sea to the Taurus Mountains, on a distance of 1000 km, and slips at a rate of $5 - 7 \text{ mm.yr}^{-1}$ (Garfunkel and Ben-Avraham, 1996, Ben-Avraham et al., 2008). The Dead Sea is one of the pull-apart basins that developed along this transpressive system.

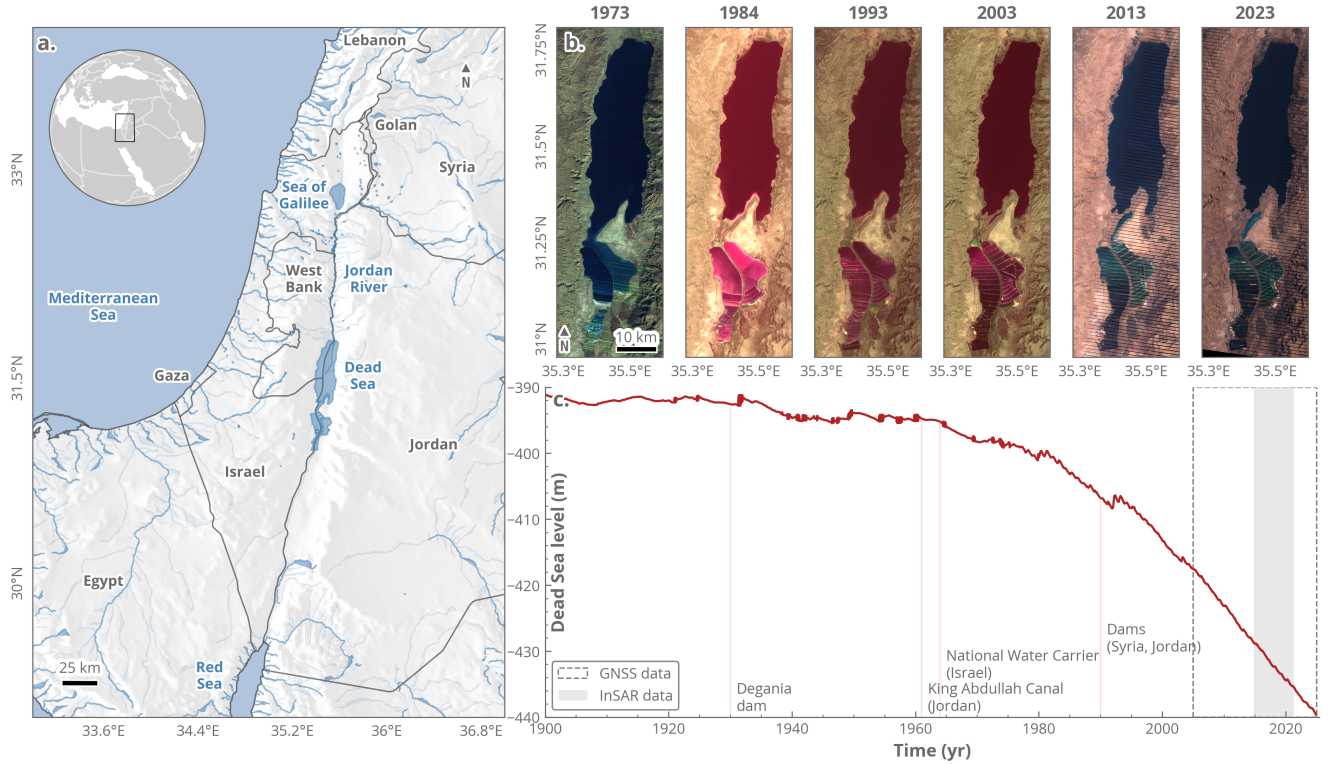


Figure 1. Framework of this study. **a.** Hydrological context of the Dead Sea. Lakes are from the HydroLAKES database (Messenger et al., 2016) and rivers from the HydroRIVERS database (Lehner and Grill, 2013). **b.** Evolution of the Dead Sea from satellite imagery (LANDSAT 1, 5 and 7) images between 1973 and 2023. **c.** Variations of the Dead Sea mean sea level since 1900. Dead Sea levels between 1900 and 1976 are from Bookman et al., 2006 and between 1976 and 2024 from the Israeli Government Water and Sewage Authority.

In 50 years, the water level in the Dead Sea has dropped by 40 m and continues to drop at a rate of 1 m.yr^{-1} (Figure 1.c). Historically, the water level of the Dead Sea remained relatively constant between 1900 and 1930. A first decrease occurred between 1930 and 1940, coinciding with an increase in the

regional population and associated water consumption. From 1940 to 1960, water levels stabilized before initiating a nearly continuous decline from the 1960s onward. This progressive drop is attributed to major human interventions, such as the construction of the Israel National Water Carrier in 1964 and Jordan's King Abdullah Canal in 1961, as well as the development of approximately 50 dams on Jordan River tributaries since the 1960s (Closson et al., 2013). In the southern sea basin, the salt and potash industries use water from the sea in evaporation ponds.

This massive and ongoing water withdrawal has multiple signatures in observed surface deformation. Locally, it produces subsidence and frequent sinkholes (Closson, 2005), while at long wavelengths, the unloading induces lithospheric rebound (Nof et al., 2012). The water level change observed in the Dead Sea may give rise to a resolvable lithospheric rebound as is observed in other areas of significant hydrological loading (Doin et al., 2015, Cavalie et al., 2007). Quantifying the hydrological deformation of the Dead Sea is essential to isolate the deformation associated with tectonic processes along the major transpressive fault system between Arabia and the Sinai microplate.

This project focuses on modelling the elastic deformation caused by the loss of water mass in the Dead Sea and comparing the results with geodetic data (GNSS and InSAR observations). Today, the Dead Sea is divided into two basins, north and south, but we will only consider the northern basin since the southern basin consists of evaporation ponds with negligible depth. We propose to model and quantify the surface deformation induced by the hydrological unloading of the Dead Sea with an elastic model and then to compare these predictions with GNSS and InSAR data.

Methodology

Modelling hydrological elastic deformation: disk loading of an elastic half-space

To model the elastic deformation fields near the Dead Sea, we begin by deriving analytical solutions for surface displacements associated with a simple disk loading assuming an elastic half-space medium. We consider a load of uniform pressure P on a disk of radius a at the surface of an elastic half-space with Young's modulus E and Poisson's ratio ν . The associated vertical and horizontal surface displacements, as derived by Johnson, 1985 and Verruijt, 2010, are:

$$u_z(r) = \begin{cases} -\frac{4(1-\nu^2)Pa}{\pi E} \mathcal{E}\left(\frac{r^2}{a^2}\right) & \text{if } r \leq a \\ -\frac{4(1-\nu^2)Pr}{\pi E} \left(\mathcal{E}\left(\frac{a^2}{r^2}\right) - \left(1 - \frac{a^2}{r^2}\right) \mathcal{K}\left(\frac{a^2}{r^2}\right) \right) & \text{if } r > a \end{cases} \quad (1)$$

$$u_r(r) = \begin{cases} -\frac{(1-2\nu)(1+\nu)}{2E} Pr & \text{if } r \leq a \\ -\frac{(1-2\nu)(1+\nu)}{2E} P \frac{a^2}{r} & \text{if } r > a \end{cases} \quad (2)$$

with u_z the vertical surface displacement, u_r the horizontal radial displacement and r the distance from the

center of the disk load. \mathcal{E} and \mathcal{K} are the complete elliptic integral of the first and second kind, respectively. For the Dead Sea, we assume that $P = \rho g \Delta h$ with $E = 100$ GPa, $\nu = 0.3$, $\rho = 1240$ $kg.m^{-3}$ the density of the Dead Sea and Δh the variation of the Dead Sea mean sea level during the study period ($\Delta h \simeq -1$ m each year in the 21th century, see Figure 1.c). Displacements due to the load on one circle are shown on Figure 2. To account for the real geometry of the Dead Sea, we discretize its shape into circles with the package `h3` (see Appendix A) and sum the displacements induced by the unloading on each circle. The shape used corresponds to the coastlines of the Dead Sea in the 1970s. We assume constant depth over the sea, without bathymetric variations.

Extraction of geodetic displacement

Surface displacements predicted by elastic modelling will be compared with two types of geodetic observations: InSAR and GNSS data. InSAR data will enable us to study spatial variations of the deformation, while GNSS data will be used to analyse temporal changes.

InSAR time series used in this study were calculated by the FLATSIM service ([Form@Ter, 2020](#), [Thollard et al., 2021](#)) using Sentinel-1 data. Calculations of the time series were made using the NSBAS interferometric processing chain ([Doin et al., 2015](#)). We only use the mean interferometric velocity in the Line-Of-Sight (LOS) of the satellite. We have an ascending track and a descending track covering the period 2015-2021. InSAR data are masked based on the number of interferograms used per pixel and network phase misclosure (Appendix B).

We use daily final GNSS solution time series processed by the Nevada Geodetic Laboratory ([Blewitt et al., 2018](#)). We select 16 stations in such way that the stations are approximately evenly distributed across the studied region. However, there is little data available for Jordan. The time series span different periods between 2005 and 2025. We correct the time series for jumps due to instrumental changes or earthquakes.

Predicted, InSAR and GNSS surface displacements are referenced to a region which is supposed to be unaffected by deformations due to the Dead Sea mass loss. This region must contain a GNSS station with good temporal coverage since it will be subtracted from the other GNSS observations. We have chosen the RAMO station which is more than 100 km south of the Dead Sea (see Figure 4) because the expected displacements due to the elastic unloading is small (Figure 2).

Results

First, we can examine the displacement results induced by the elastic unloading on a simple disk. Figure 2.a-b shows the deformation resulting from a 15 km-radius disk uniformly unloaded with 10 m of water (corresponding roughly to the decline of the Dead Sea water level during 10 years). The surface of this disk corresponds to the surface of the Dead Sea (~ 605 km^2). The predicted displacements are between 0 and 20 mm beyond the disk for a period corresponding to approximately 10 years. The displacements extend beyond the unloaded region with the maximum vertical and horizontal displacements occurring at the center of the disk and at the load boundary, respectively. The horizontal displacements are much smaller than the vertical displacements (around four times less at the load boundary).

Second, we can examine the displacements induced by the elastic discharge on a realistic geometry of the Dead Sea. Figure 2.c-d shows the deformation resulting from the Dead Sea uniformly unloaded with 10 m of water. The structure of the surface displacements is similar to that of a simple disk. Predicted displacements decrease significantly with distance from the Dead Sea; between the coast and 50 km from the coast, vertical displacements fall from 16 mm to 4 mm and horizontal displacements from 4 mm to 1 mm. The predicted horizontal and vertical displacements are higher along the east and west coasts than along the north and south coasts. The expected signals are of low amplitude (of the order of a mm or 10 mm). Signals of such low amplitudes are difficult to detect with InSAR, so we expect them to be better observed with GNSS.

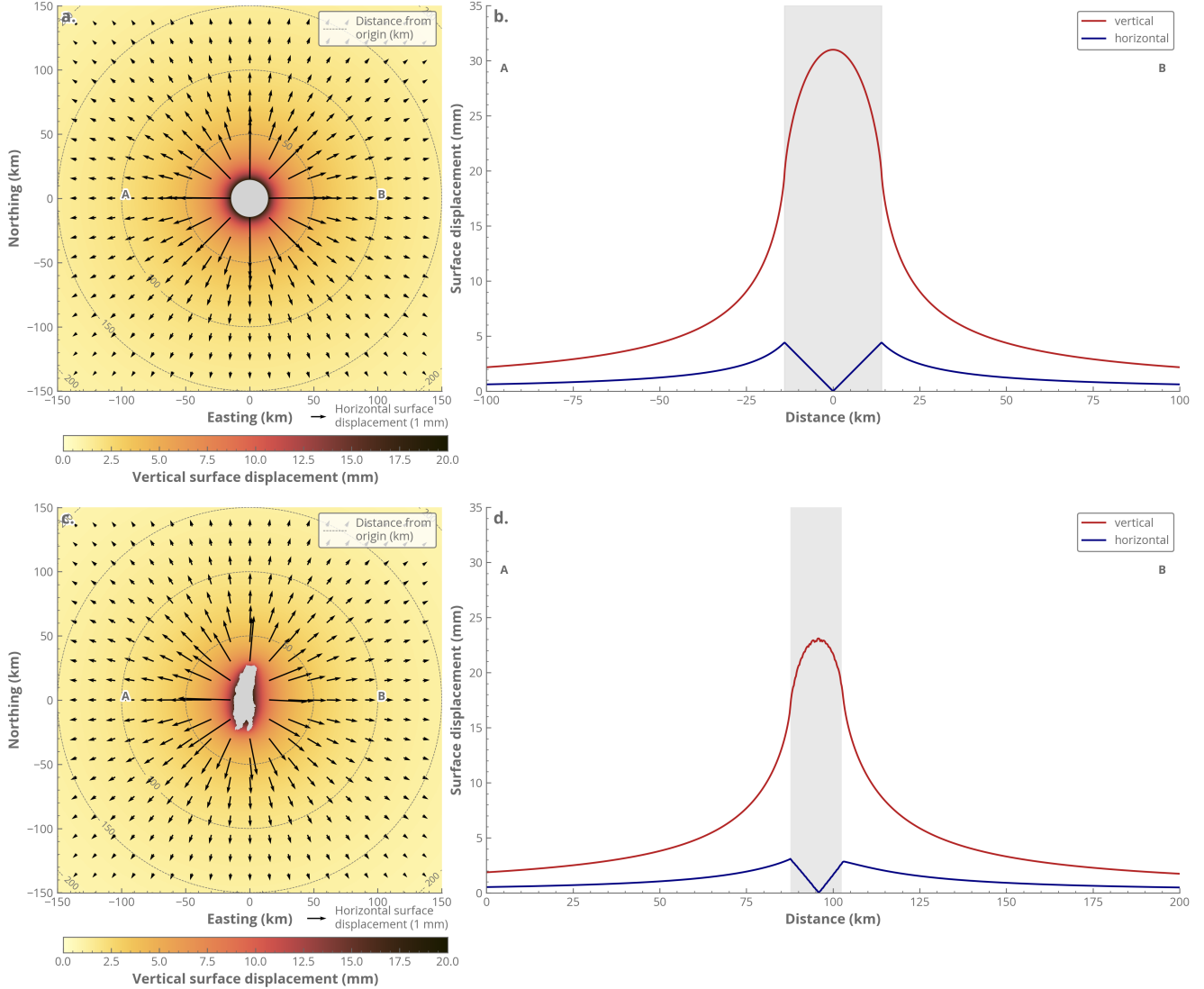


Figure 2. Predicted surface displacements due to hydrological elastic unloading on a disk of radius $a = 15$ km (a. and b.) or on the Dead Sea (c. and d.) with a decline of the Dead Sea water level of $\Delta h = -10$ m. b. and d. show profiles between points A and B. The gray-shaded area indicates the disk or the Dead Sea.

We compare our elastic unloading predictions with InSAR displacement velocities. For each track, we calculate the theoretical displacement velocities for a Dead Sea water level decrease of $\Delta h = -6.7$ m

which corresponds to the InSAR time series period (2015-2021). The velocities are then projected into the LOS. The data, the predictions and the residuals are shown on Figure 3 for the ascending track and the descending track. The InSAR displacement velocities show an uplift around the Dead Sea (of the order of 2 mm.yr^{-1} at the coast), which is more visible for the ascending track. This uplift is predicted by our elastic model. However, the predicted displacement is of lower amplitude (of the order of 1.25 mm.yr^{-1} at the coast). We observe a residual uplift after subtracting the prediction (of the order of 0.75 mm.yr^{-1} at the coast). This suggests that the elastic model cannot explain all the observed deformation and that other phenomena need to be taken into account. The comparison is complicated by the fact that there is little data very close to the coast of the Dead Sea. This is where the elastic deformation should be concentrated according to our modelling.

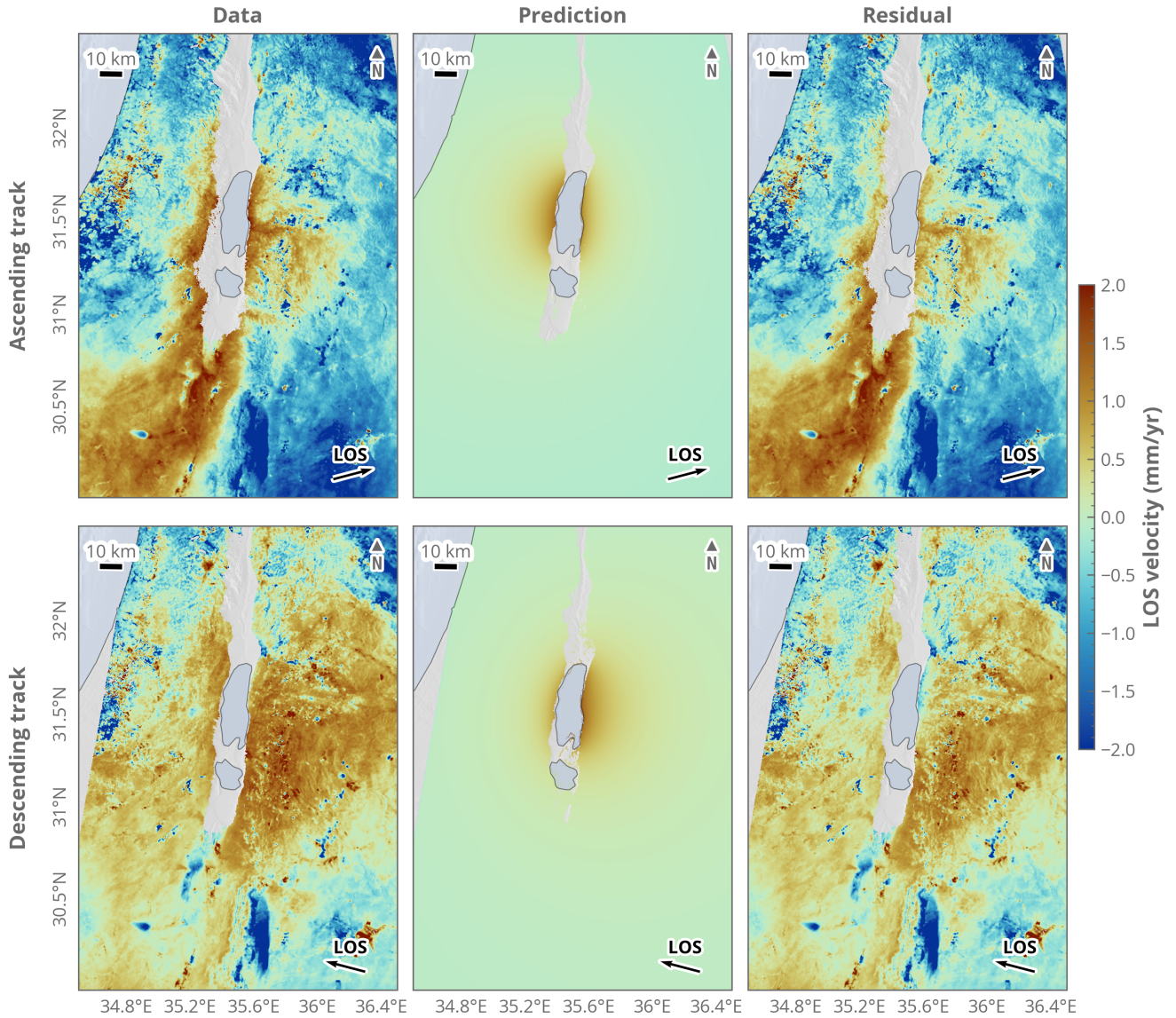


Figure 3. LOS surface displacement velocity for the period 2015-2021 from InSAR time series (left) and elastic unloading model (middle). Residuals between the data and the predictions are shown on the left. Displacements are referenced to the GNSS station RAMO (see Figure 4).

Comparing the predictions with the InSAR data allows us to see the consistency of our predictions on

a spatial scale, although they do not fully explain the data. We compare our predictions with GNSS data to assess the temporal consistency of our predictions. The GNSS time series span different periods between 2005 and 2025. We calculate the theoretical displacement time series at each GNSS stations using the Dead Sea water level time series (Figure 1.c). To compare all the stations, we calculate the average displacement velocities at each station based on observations or predictions. The data and the predictions are shown on Figure 4. For horizontal components, the predicted displacements are much smaller than those observed (at least 10 times smaller). The horizontal GNSS velocities do not show the expected structure predicted by elastic modelling (Figure 2.c). The tectonic component still seems to appear in the horizontal velocities. A correction using a plate motion model might improve the separation of non-tectonic signals. For the vertical component, apart from the MAS5, UJAP and BALJ stations, the observed and predicted displacements are of the same order of magnitude. In the direct vicinity of the Dead Sea, only DRAG shows a similarity between prediction and observation. Overall, the results are less consistent between predictions and GNSS observations than with InSAR. The observed displacements are sensitive to the displacements of the RAMO station used as a reference.

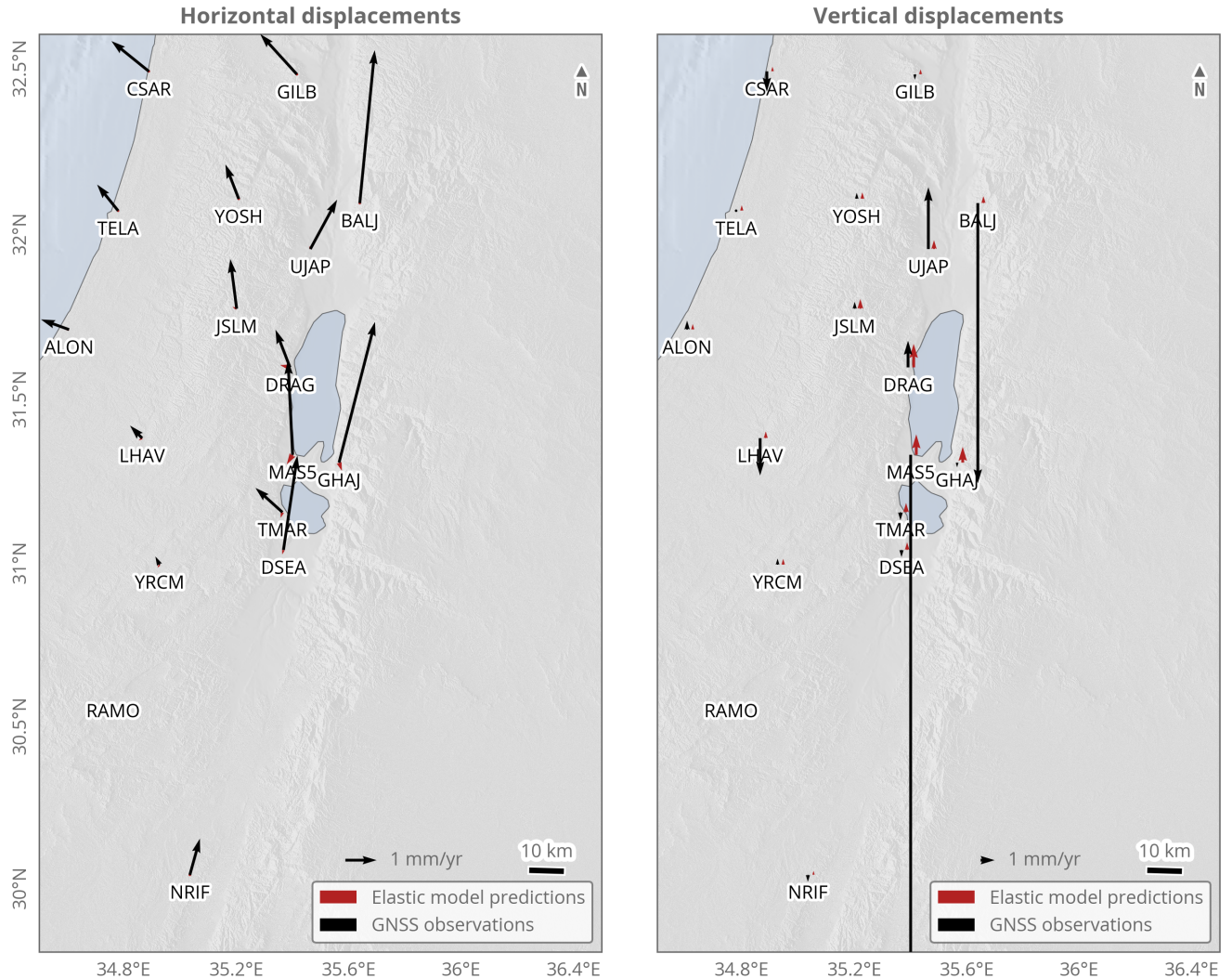


Figure 4. Surface displacement velocity from GNSS data or elastic modelling. At station MAS5, the observed vertical velocity is -56 mm.yr^{-1} . Displacements are referenced to the GNSS station RAMO.

Finally, we compare GNSS displacement time series with modelled displacement time series at one GNSS station (Figure 5). We choose the station DRAG which is on the western coast of the Dead Sea because of its good temporal coverage and because the expected deformation signals are stronger in the vicinity of the Dead Sea. The other stations are shown in Appendix C. For vertical displacement, observations and predictions show an uplift that is slightly more marked in the data (40 mm observed in 20 years compared with 30 mm predicted). For the horizontal displacement, the eastern component is well reproduced by the model, but the station shows a strong northward displacement that is not explained by the elastic model (25 mm in 20 years compared with 2 mm predicted). Displacements at a GNSS station may be influenced by local factors that have not been modelled. The predictions show little or no seasonal oscillation.

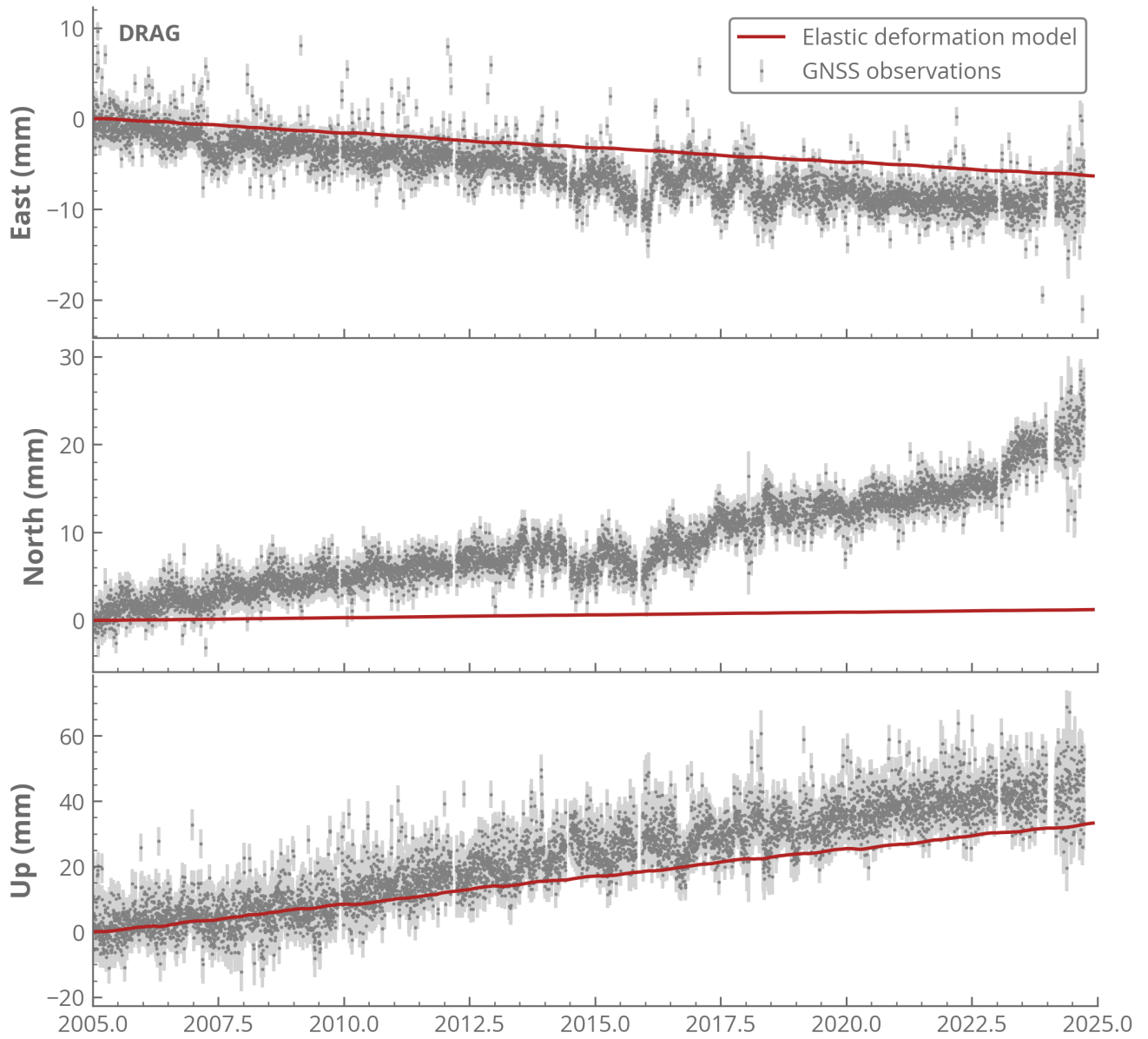


Figure 5. Surface displacement time series at the GNSS station DRAG (see map on Figure 4). Observed GNSS data and predictions from the elastic unloading model are shown.

Discussion

The goal of this work was to model the deformations due to the decline of the Dead Sea water level. We focused on modelling the elastic unloading and comparing our predictions with GNSS and InSAR data. The expected ground displacement was estimated to be a few millimeters per year. Our results show that the elastic model does not fully explain the observed surface deformations.

In this project, we model the crust as being homogeneous and behaving only elastically. This approximation generally holds when studying deformation of the upper crust. However, our preliminary results indicate that the elastic surface displacements due to the unloading is less important than the observed surface displacements. This suggests that elastic deformation alone is not sufficient to explain the observed crustal behavior, highlighting the need for considering additional mechanisms. [Nof et al., 2012](#) modelled the total surface deformation around the Dead Sea using a purely elastic model but with a Young's modulus of 44 GPa.

For us, one possibility is to include visco-elastic deformation to capture the complexity of crustal deformation. It is reasonable to think that viscous deformation is occurring because the characteristic spatial wavelength of the elastic deformation is of the order of 50 km (Figure 2), which suggests a response from the upper mantle. Modelling the visco-elastic deformation would require using the entire Dead Sea water level time series since the beginning of the 20th century.

Furthermore, the crust is not homogeneous in its composition. Variations in material properties, such as the presence of aquifers, can significantly influence how it deforms. To account for these variations, a poro-elastic model could be used to model the aquifers. Groundwater can play a role in the observed surface deformation, depending on the size of the aquifer system and associated volumes, its connectivity to the surface and whether it also loses water. In addition, the rheological properties of the underground were considered to be constant. We could consider stratified models for Young's modulus, for example.

In addition to these models of crustal response, other factors associated with the decrease in the Dead Sea water level must also be considered. We could correct the Dead Sea water level time series for steric sea level variations which are variation of the sea volume due to density changes (expansion or contraction of water masses), through salinity and temperature variations.

On a larger scale, hydrological changes across the entire region also contribute to crustal deformation. Such deformations must be carefully distinguished from those caused directly by the drop in the Dead Sea water level. One way to address this is by using data from the GRACE satellite mission, which provides information about large-scale hydrological changes.

Conclusion and perspectives

This project presents a detailed analysis of the vertical and horizontal elastic deformation induced by the decrease in the Dead Sea water level. Using data from InSAR and selected GNSS sites, we compare the observed deformation with predictions from our elastic deformation model. The comparison indicates that while our elastic model captures some aspects of the observed deformation, it is not comprehensive enough

to fully describe the deformation. This highlights the need to consider additional models and variables to build a more accurate representation.

Future work should focus on refining deformation modelling, using visco-elastic models or poro-elastic models, and taking into account steric effects. Comparison with the data can be improved by using a plate motion model correction and removing the deformation due to large-scale hydrological mass redistribution. Accurately estimating the deformation could help infer rheological properties of the underground or estimate the water content of aquifer near the Dead Sea.

Acknowledgements and reproducibility

The authors would like to thank Manon Dalaison and Kristel Chanard for their availability and reactivity in supervising this tutored project, and for their guidance and help during these two months. The codes used for this project are freely available at https://github.com/emile-dns/dead_sea_tutored_project.git.

References

- Ben-Avraham, Z., Garfunkel, Z., & Lazar, M. (2008). Geology and Evolution of the Southern Dead Sea Fault with Emphasis on Subsurface Structure [Publisher: Annual Reviews]. *Annual Review of Earth and Planetary Sciences*, 36, 357–387. <https://doi.org/10.1146/annurev.earth.36.031207.124201>
- Blewitt, G., Hammond, W. C., & Kreemer, C. (2018). Harnessing the GPS data explosion for interdisciplinary science. *Eos*, 99. <https://doi.org/https://doi.org/10.1029/2018EO104623>
- Bookman, R., Bartov, Y., Enzel, Y., & Stein, M. (2006, January 1). Quaternary lake levels in the Dead Sea basin: Two centuries of research. In Y. Enzel, A. Agnon, & M. Stein (Eds.), *New Frontiers in Dead Sea Paleoenvironmental Research* (p. 0). Geological Society of America. [https://doi.org/10.1130/2006.2401\(10\)](https://doi.org/10.1130/2006.2401(10))
- Cavalié, O., Doin, M.-P., Lasserre, C., & Briole, P. (2007). Ground motion measurement in the Lake Mead area, Nevada, by differential synthetic aperture radar interferometry time series analysis: Probing the lithosphere rheological structure. *Journal of Geophysical Research: Solid Earth*, 112. <https://doi.org/10.1029/2006JB004344>
- Closson, D. (2005). Structural control of sinkholes and subsidence hazards along the Jordanian Dead Sea coast. *Environmental Geology*, 47(2), 290–301. <https://doi.org/10.1007/s00254-004-1155-4>
- Closson, D., Pasquali, P., Riccardi, P., Milisavljevic, N., & Abou Karaki, N. (2013, January). The water deficit in The Middle East and The Disappearance of the Dead Sea. In *Desertification and Land Degradation Processes and Mitigation* (First). Unesco Chair of Eremology.
- Doin, M.-P., Twardzik, C., Ducret, G., Lasserre, C., Guillaso, S., & Jianbao, S. (2015). InSAR measurement of the deformation around Siling Co Lake: Inferences on the lower crust viscosity in central Tibet. *Journal of Geophysical Research: Solid Earth*, 120(7), 5290–5310. <https://doi.org/10.1002/2014JB011768>
- Form@Ter. (2020). FLATSIM Data Products: Data Products generated by FLATSIM (ForM@Ter LArge-scale multi-Temporal Sentinel-1 InterferoMetry). <https://doi.org/10.24400/253171/FLATSIM2020>

- Garfunkel, Z., & Ben-Avraham, Z. (1996). The structure of the Dead Sea basin. *Tectonophysics*, 266(1), 155–176. [https://doi.org/10.1016/S0040-1951\(96\)00188-6](https://doi.org/10.1016/S0040-1951(96)00188-6)
- Johnson, K. L. (1985). *Contact Mechanics*. Cambridge University Press. <https://doi.org/10.1017/CBO9781139171731>
- Lehner, B., & Grill, G. (2013). Global river hydrography and network routing: baseline data and new approaches to study the world's large river systems. *Hydrological Processes*, 27(15), 2171–2186. <https://doi.org/10.1002/hyp.9740>
- Messager, M. L., Lehner, B., Grill, G., Nedeva, I., & Schmitt, O. (2016). Estimating the volume and age of water stored in global lakes using a geo-statistical approach [Publisher: Nature Publishing Group]. *Nature Communications*, 7(1), 13603. <https://doi.org/10.1038/ncomms13603>
- Nof, R. N., Ziv, A., Doin, M.-P., Baer, G., Fialko, Y., Wdowinski, S., Eyal, Y., & Bock, Y. (2012). Rising of the lowest place on Earth due to Dead Sea water-level drop: Evidence from SAR interferometry and GPS. *Journal of Geophysical Research: Solid Earth*, 117. <https://doi.org/10.1029/2011JB008961>
- Thollard, F., Clesse, D., Doin, M.-P., Donadieu, J., Durand, P., Grandin, R., Lasserre, C., Laurent, C., Deschamps-Ostanciaux, E., Pathier, E., Pointal, E., Proy, C., & Specht, B. (2021). FLATSIM: The ForM@Ter LArge-Scale Multi-Temporal Sentinel-1 InterferoMetry Service [Number: 18 Publisher: Multidisciplinary Digital Publishing Institute]. *Remote Sensing*, 13(18), 3734. <https://doi.org/10.3390/rs13183734>
- Verruijt, A. (2010). Elastostatics of a Half Space. In A. Verruijt (Ed.), *An Introduction to Soil Dynamics* (pp. 157–186). Springer Netherlands. https://doi.org/10.1007/978-90-481-3441-0_8

Appendices

A Discretization of the Dead Sea geometry

To account for the real geometry of the Dead Sea in the modelling of elastic deformation, we discretize the shape of the Dead Sea into circles. We use the package `h3` to discretize a polygon into 770 hexagons and then fill the hexagons with circles of constant radius ($a = 461.3\text{ m}$). The mesh is shown on Figure 6.

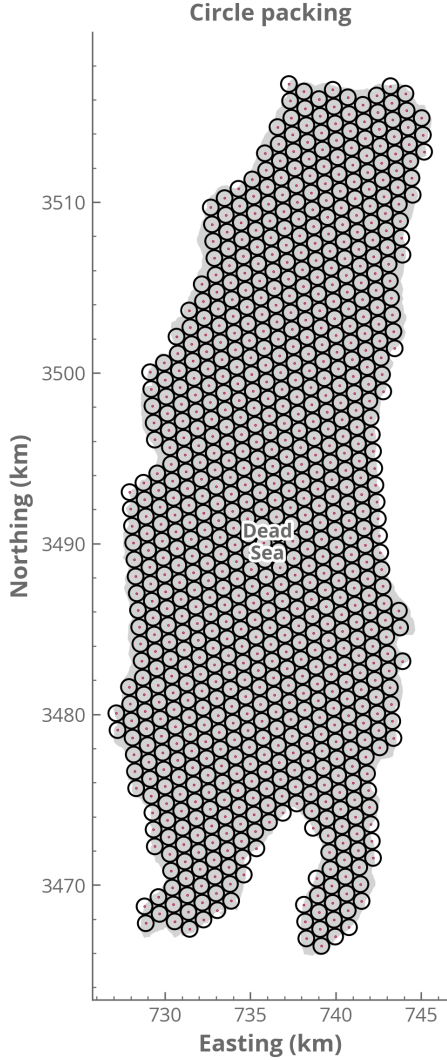


Figure 6. Discretization of the Dead Sea used to model the elastic deformation.

B Description of the InSAR data

InSAR displacement velocities were masked to take into account quality scores for the time series. Figure 7 shows the LOS surface displacement velocities, the number of interferograms used per pixel, the network misclosure per pixel and the temporal coherence. The distributions of these variables are also shown, they were used to establish thresholds for the masks. Pixels with less than 100 interferograms were masked as well as pixels with a network misclosure higher than 0.8.

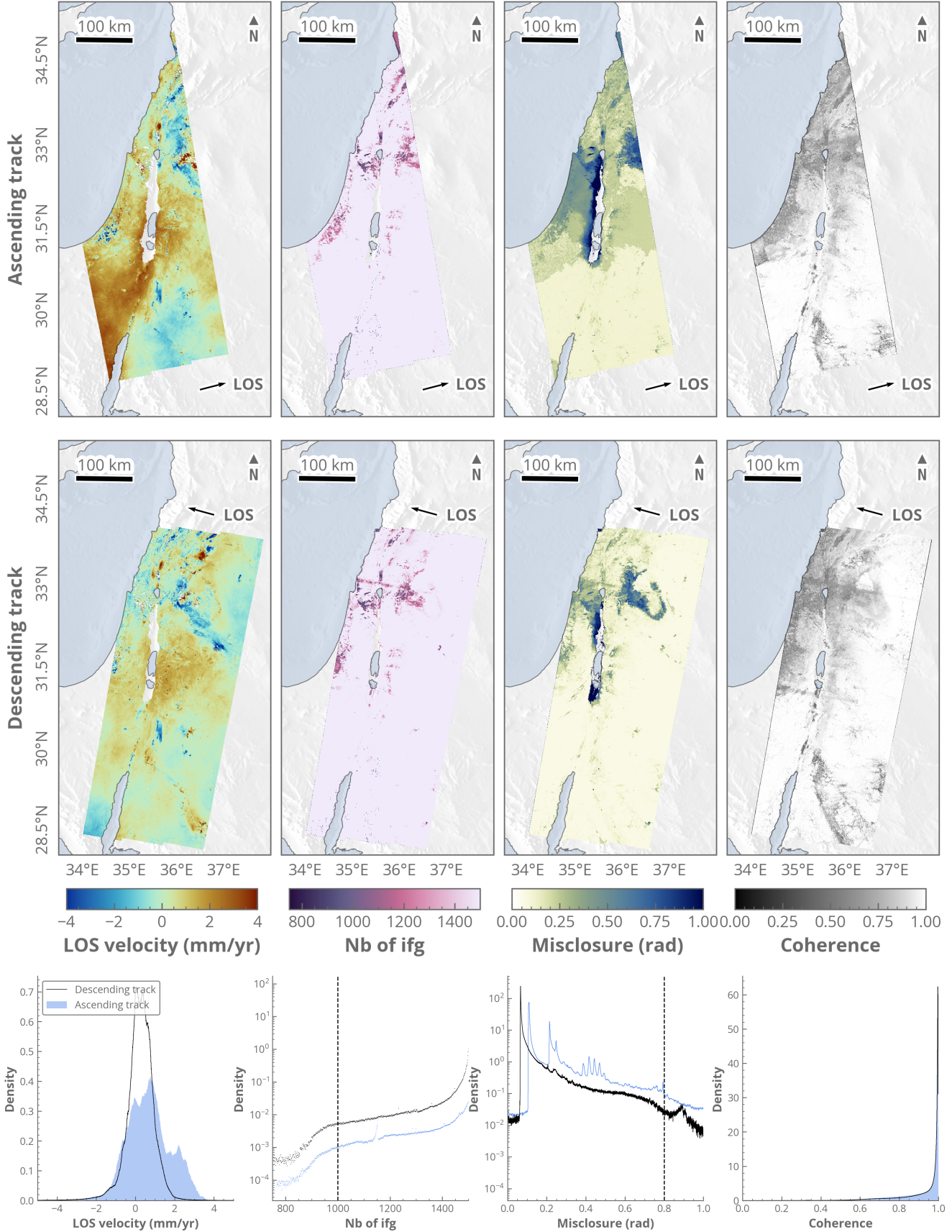


Figure 7. InSAR LOS velocities, number of interferograms used, network misclosure and temporal coherence for each InSAR track. Dashed lines on the distributions show the threshold used for masking.

C Displacement time series at GNSS stations

